BIOCHEMISTRY

 Volume 43, Number 39 October 5, 2004

Articles

Negatively Charged Residues and Hydrogen Bonds Tune the Ligand Histidine pK_a Values of Rieske Iron−Sulfur Proteins†

Astrid R. Klingen and G. Matthias Ullmann*

Department of Structural Biology/Bioinformatics, Bayreuth University, Universitätsstrasse 30, BGI, D-95447 Bayreuth, Germany

Received June 3, 2004; Revised Manuscript Received July 27, 2004

ABSTRACT: Rieske proteins carry a redox-active iron−sulfur cluster, which is bound by two histidine and two cysteine side chains. The reduction potential of Rieske proteins depends on pH. This pH dependence can be described by two pK_a values, which have been assigned to the two iron-coordinating histidines. Rieske proteins are commonly grouped into two major classes: Rieske proteins from quinol-oxidizing cytochrome *bc* complexes, in which the ligand histidines titrate in the physiological pH range, and bacterial ferredoxin Rieske proteins, in which the ligand histidines are protonated at physiological pH. In the study presented here, we have calculated pK_a values of the cluster ligand histidines using a combined density functional theory/continuum electrostatics approach. Experimental pK_a values for a *bc*-type and a ferredoxin Rieske protein could be reproduced. We could identify functionally important differences between the two proteins: hydrogen bonds toward the cluster, which are present in *bc*-type Rieske proteins, and negatively charged residues, which are present in ferredoxin Rieske proteins. We removed these differences by mutating the proteins in our calculations. The Rieske centers in the mutated proteins have very similar pK_a values. We thus conclude that the studied structural differences are the main reason for the different pH-titration behavior of the proteins. Interestingly, the shift caused by neutralizing the negative charges in ferredoxin Rieske proteins is larger than the shift caused by removing the hydrogen bonds toward the cluster in *bc*-type Rieske proteins.

Rieske proteins are redox-active iron−sulfur proteins (*1*). The iron−sulfur cluster common to all Rieske proteins consists of an [Fe_2S_2] core with two histidine side chains as ligands to one iron ion and two cysteine side chains as ligands to the other iron ion (see Figure 1). In the oxidized state of the cluster, both irons are in their Fe(III) state.

Rieske proteins display a characteristic pH-titration behavior that can be described by two pK_a values, which depend on the redox state of the cluster. These pK_a values were assigned to the two iron-coordinating histidine side chains (*2*−*5*). The pK_a values are lower for the oxidized than for

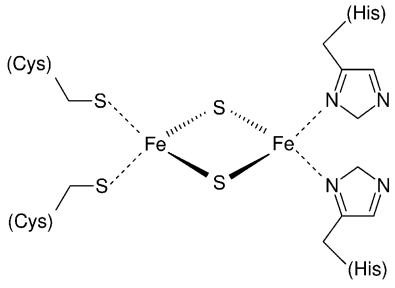

FIGURE 1: The chemical structure of the Rieske iron−sulfur cluster. The [Fe_2S_2] core and coordinating histidine and cysteine side chains are shown.

† This work was supported by Grant UL174/2 of the Deutsche Forschungsgemeinschaft and a travel grant of BaCaTec. A.R.K. thanks the Boehringer Ingelheim Fonds for a doctoral fellowship.

* To whom correspondence should be addressed. Phone: +49-921-553545. Fax: +49-921-553544. E-mail: matthias.ullmann@uni-bayreuth.de.

10.1021/bi0488606 CCC: $27.50
Published on Web 09/11/2004

the reduced state of the cluster. Thus, reduction of the cluster favors protonation of the ligand histidines. The redox-dependent pK_a values of Rieske proteins describe the pH dependence of their reduction potentials.

On the basis of their catalytic function and chemical properties, Rieske proteins are commonly grouped into two classes (*6*, *7*). Rieske proteins of the first class are part of membrane-bound quinol-oxidizing complexes such as cytochrome bc_1 and cytochrome b_6f. These *bc*-type Rieske proteins have pH-dependent reduction potentials. Their reduction potentials at pH = 7 vary between 150 and 400 mV depending on the type of quinol they react with. In the oxidized state, one of the pK_a values of the ligand histidines of *bc*-type Rieske proteins lies in the physiological pH range, while both histidines are protonated if the cluster is reduced. Rieske proteins of the second class, in the following called ferredoxin Rieske proteins, take part in oxidative hydroxylation of aromatic compounds. They have reduction potentials of about −150 mV at pH = 7 that are pH-dependent only above the physiological pH range. Irrespective of the redox state of the cluster, ligand histidines in ferredoxin Rieske proteins are protonated under physiological conditions.

In the study presented here, we have calculated pK_a values of a *bc*-type and a ferredoxin Rieske protein. We identified differences in the electrostatics of the two proteins that account for the observed difference between their pK_a values. The investigated proteins are the Rieske protein from a mitochondrial cytochrome bc_1 complex (*8*), in the following abbreviated as bc1R,[1] and a bacterial ferredoxin Rieske protein (*7*), in the following abbreviated as FdR. In the next section, we provide some theoretical background on the calculation of pK_a values in proteins by a combined density functional theory/continuum electrostatics approach. Results are presented for the wild-type structures of the two Rieske proteins, as well as for mutated structures. The analysis of the behavior of the mutants reveals that differences in the hydrogen bond pattern and, more importantly, differences in the distribution of negatively charged residues between bc1R and FdR are responsible for the difference in the pH dependence of their reduction potentials.

THEORETICAL BACKGROUND AND COMPUTATIONAL DETAILS

Calculation of pK_a Values. The protonation equilibrium $HA \rightleftharpoons A^- + H^+$ is described by its equilibrium constant, $K_a = ([A^-][H^+])/[HA]$, and its $pK_a = -\log K_a$. The titration behavior of the same group in solution and a protein environment can differ considerably (*9*−*11*). A shift in the pK_a value may be introduced by a change in the dielectric environment and by the interaction with nontitratable background charges in the protein. In addition, the protonation probability of the respective group can depend on the state of other titratable groups. This interaction can change the profile of the titration curve.

To calculate pK_a values of the iron-coordinating histidines in different Rieske protein environments, we make use of the thermodynamic cycle depicted in Figure 2. The deprotonation energy in vacuum ΔG^{vac}_{deprot} can be obtained from density functional theory (DFT) calculations. The energies to transfer different states of the titratable group from vacuum to the protein environment are calculated by a continuum electrostatics approach. The transfer energy of a proton $\Delta G_{trans}(H^+) = -260.5$ kcal/mol is calculated from the experimentally determined reduction potential of the standard hydrogen electrode (*12*). Combining the results from DFT and continuum electrostatics calculations (*13*), we obtain the deprotonation energy in the protein environment as

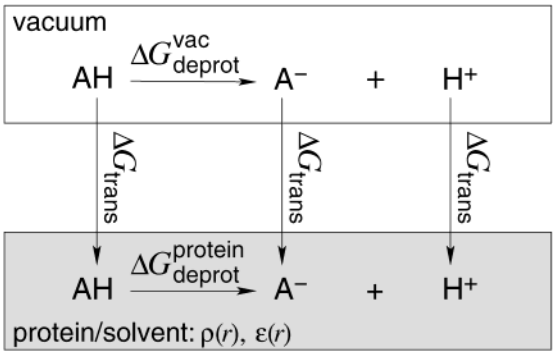

FIGURE 2: Thermodynamic cycle to calculate the deprotonation energy in a protein $\Delta G^{protein}_{deprot}$. The protein/solvent environment is characterized by a spatial distribution of partial charges $\rho(r)$ and dielectric boundaries $\epsilon(r)$. The energies to transfer the species AH and A^- from vacuum to the protein are obtained from continuum electrostatics calculations solving the Poisson−Boltzmann equation. The energy of deprotonation in vacuum ΔG^{vac}_{deprot} is obtained from density functional calculations.

$$\Delta G^{protein}_{deprot} = \Delta G^{vac}_{deprot} + \Delta G_{trans}(A^-) + \Delta G_{trans}(H^+) - \Delta G_{trans}(AH) \quad (1)$$

The resulting energies represent relative energies of protonation microstates. The corresponding microscopic pK_a values are given by $pK_a = (RT \ln 10)^{-1}\Delta G^{protein}_{deprot}$. The microscopic p$K_a$ values describe the conversion between different microstates of the cluster as depicted in Figure 3 but do not correspond to the observables in, for instance, potentiometric experiments. Such experimentally accessible macroscopic pK_a values can yet be calculated from the microscopic pK_a values obtained from DFT and continuum electrostatics calculations. In its oxidized state, the Rieske cluster is an example of a diprotic acid. The macroscopic equilibrium constants of the deprotonation reactions of the ligand histidines can thus be calculated by (*14*, *15*)

$$K^{ox1}_{mac} = K^{ox}_{11} + K^{ox}_{12} \qquad \text{and}$$

$$K^{ox2}_{mac} = \frac{K^{ox}_{12}K^{ox}_{22}}{K^{ox}_{12} + K^{ox}_{22}} \quad (2)$$

The meaning of the different microscopic equilibrium constants K^{ox} is equivalent to the pK_a values in Figure 3. The macroscopic equilibrium constants K_{mac} correspond directly to the equilibrium constants in the fitting procedure applied by Zu et al. when measuring pH-dependent reduction potentials of Rieske centers (*16*).

To calculate macroscopic pK_a values for the reduced state of the cluster, a total of eight microstates must be considered. Our DFT calculations differentiate between states with the

[1] Abbreviations: bc1R, Rieske protein from bovine mitochondrial cytochrome bc_1 complex; FdR, bacterial ferredoxin Rieske protein; DFT, density functional theory.

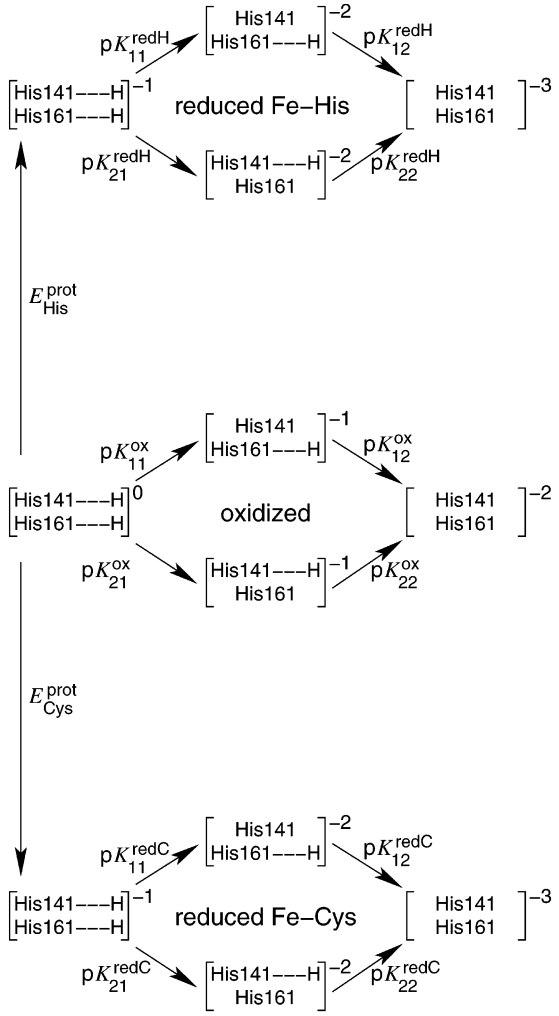

FIGURE 3: Twelve possible microstates of the Rieske cluster and their interconversion. Numbering of ligand histidines corresponds to the bc1R sequence. The electron can formally reduce either the histidine-coordinated iron (reduced Fe−His) or the cysteine-coordinated iron (reduced Fe−Cys). For each of the three different redox states, there are four protonation states: both histidines can be protonated, His141 protonated and His161 deprotonated, His141 deprotonated and His161 protonated, or both histidines deprotonated. The net charges of the cluster (iron−sulfur core with ligand side chains) are given.

reducing electron formally placed at the histidine-coordinated iron and states with the reducing electron formally placed at the cysteine-coordinated iron. Experimentally these states are not distinguished since they may both form when the cluster gets reduced. The equations for obtaining macroscopic pK_a values of the reduced state are in principle analogous to eq 2; they are, however, more complicated. Together with a detailed derivation, these equations are given in the Supporting Information.

Density Functional Theory Calculations. DFT calculations were performed with the Amsterdam Density Functional program suite (ADF 2000.02, functionals VWN and PW91, see refs *17*−*19*). Input coordinates for the DFT calculations were taken from the bc1R crystal structure (*8*). The calculations were performed as described in a previous paper (*5*); however, the hydroxyl groups of Ser163 and Tyr165 were excluded. The cluster was geometry-optimized in the 12 different states shown in Figure 3. Partial charges were derived from the DFT calculation results by a CHELPG-based algorithm (*20*) combined with singular value decomposition (*21*). Atom radii published by Bondi (*22*) were used in the fitting procedure.

The deprotonation energy in vacuum as depicted in Figure 2 was calculated as

$$\Delta G_{deprot}^{vac} = H_{DFT}(A^-) + H_{DFT}(H^+) - H_{DFT}(AH) + H_{vib}(A^-) - H_{vib}(AH) + H_{translation}(H^+) + \Delta(pV) - TS(H^+) \quad (3)$$

H_{DFT} are the absolute energies of the respective species obtained from the DFT calculations, H_{vib} are the vibrational energies derived from normal-mode analysis of methylimidazole (*5*), $H_{translation}(H^+) = {}^3/_2RT$ is the translational energy of a proton, $\Delta(pV) = RT$ is the energy change during deprotonation due to the change in volume, and $TS(H^+) = 7.8$ kcal/mol is the entropic contribution derived from the Sackur−Tetrode equation (*23*). R is the universal gas constant, and T is the temperature.

Preparation of the Crystal Structures for Continuum Electrostatics Calculations. The studied proteins, named bc1R and FdR, respectively, are the soluble domain of the Rieske protein from bovine mitochondrial cytochrome bc_1 complex (PDB-code 1RIE, 1.5 Å resolution, see ref *8*) and the ferredoxin Rieske protein from the biphenyl dioxygenase system in *Burkholderia* sp. (PDB-code 1FQT, 1.6 Å resolution, see ref *7*). FdR has been crystallized as a dimer, and both monomers contain residues modeled in alternative conformations (*7*). Calculations were performed separately on alternative structures of both monomers, and obtained pK_a values differ by less than 0.3 pK units. Since monomer B (see 1FQT.pdb, ref *7*) contained less residues modeled in alternative conformations than monomer A, results obtained for this monomer are presented in this paper.

The crystal structures were prepared for the electrostatics calculations using the CHARMM program package (*24*). Hydrogen atom positions were constructed and subsequently energy-minimized. Mutations were introduced by changing the respective side chains, while leaving the positions of all unchanged atoms fixed.

Continuum Electrostatics Calculations. Optimized geometries and partial charges of the different cluster states were obtained from the DFT calculations. These geometries and charges were the basis for the calculation of histidine pK_a values in the different protein environments (*13*). The transfer energies illustrated in Figure 2 have two major contributions. The Born energy contribution arises from the change in dielectric environment between vacuum ($\epsilon_{vacuum} = 1$) and the protein/solvent environment ($\epsilon_{protein} = 4$ and $\epsilon_{solvent} = 80$). The so-called background energy is due to the interaction of the cluster with the charge distribution of the protein/solvent environment. Both the Born and the background energy are obtained by calculating the energy of the charge distribution of the cluster in the electrostatic potential of the protein/solvent environment (*5*, *9*). Structural changes of the protein due to the changed charge distribution of the cluster are not included in the calculations. The electrostatic potential of the protein as a function of the dielectric boundary and charge distributions is calculated by solving the linearized Poisson−Boltzmann equation using the MEAD program package (*25*). In the Poisson−Boltzmann calculation, the

Table 1: Calculated Macroscopic pK_a values for Wild-Type bc1R and FdR in Comparison with Experimental Data

	pK_a values			
	oxidized		reduced	
calculated bovine bc1R	7.9	9.2	10.8	13.7
experimental bovine bc1R (*26*)	7.7	9.1	>10.6	>10.6
experimental *Rhodobacter* bc1R (*16*)	7.6 ± 0.1	9.6 ± 0.1	12.4 ± 0.4	12.4 ± 0.4
calculated FdR	9.1	9.8	12.2	14.5
experimental FdR (*16*)	9.8 ± 0.2	11.5 ± 0.4	13.3 ± 0.8	13.3 ± 0.8

ionic strength of the solvent is set to the physiological value of 0.15 M. The protein is described by partial charges from the CHARMM22 parameter set (*24*) and atom radii published by Bondi (*22*).

RESULTS AND DISCUSSION

Ligand Histidine pK_a Values in the Wild-Type Structures of bc1R and FdR. We have calculated pK_a values of the ligand histidines in the wild-type structures of the two different Rieske proteins using the described combined DFT/continuum electrostatics approach. Table 1 lists calculated and experimentally determined macroscopic pK_a values of the ligand histidines in wild-type bc1R and FdR. We obtain very good agreement with pK_a values determined experimentally for bovine bc1R (*26*). Agreement with values obtained for the same protein from *Rhodobacter sphaeroides* (*16*) is good for the oxidized state of the cluster. For the reduced state of the cluster, experimental data for *Rb. sphaeroides* and calculated data for the bovine enzyme differ. This discrepancy may be due to structural instability of the Rieske protein at the high pH values applied in the experiment. Instabilities of the Rieske protein from the cytochrome bc_1 complex at high pH values have previously been observed spectroscopically (*27*).

Comparison of experimental and calculated pK_a values for FdR from *Burkholderia* (*16*) shows reasonable agreement for the oxidized state. Differences for the reduced state of the cluster can be explained in the same way as for the comparison of bovine and *Rb. sphaeroides* bc1R. Since a common overall topology has been observed in all Rieske proteins (*7*, *8*, *28*−*32*), the structural changes observed for a *bc*-type Rieske protein occur most likely also in FdR. In addition, Zu et al. report some uncertainty in the fit yielding two identical pK_a values for the reduced cluster (*16*).

Physical Basis of the Difference in pK_a Values between bc1R and FdR. In the calculations, we obtained higher histidine pK_a values for FdR than for bc1R as observed experimentally. To understand the physical basis of the difference between the pK_a values, we have further analyzed the results from the Poisson−Boltzmann calculations. In our calculations, any difference between obtained pK_a values in the two proteins is due to differences in the transfer energy of the microstates from vacuum to the respective protein environment (see Figure 2). A decomposition of the transfer energies, ΔG_{trans}, of four different microstates of the cluster into the Born energy, ΔG_{Born}, and the background energy, ΔG_{back}, is shown in Table 2.

For both protein environments, the transfer energy gets more negative with an increasing charge of the cluster (from oxidized and protonated, 0, to reduced and doubly deprotonated, −3). This effect is mainly due to an increase in ΔG_{Born}, while ΔG_{back} shows no dependence on the cluster charge. The general charge-stabilizing effect of the higher dielectric of the protein compared to vacuum is more pronounced for the cluster states with a high charge density. In all cases, the Born energy contributes most to the transfer energy.

Table 2: Decomposition of the Transfer Energy (see Figure 2) as Obtained from the Poisson−Boltzmann Calculations: $\Delta G_{trans} = \Delta G_{Born} + \Delta G_{back}$[a]

		microstate energies [kcal/mol]			
energy terms		ox, prot	redH, prot	ox, deprot	redH, deprot
ΔG_{trans}	bc1R	−60.7	−94.6	−165.4	−313.9
	FdR	−52.4	−81.3	−154.0	−297.6
	ΔΔ	8.3	13.3	11.4	16.3
ΔG_{Born}	bc1R	−48.4	−77.1	−150.4	−294.1
	FdR	−48.3	−77.0	−150.3	−293.8
	ΔΔ	0.1	0.1	0.1	0.3
ΔG_{back}	bc1R	−12.3	−17.5	−15.0	−19.9
	FdR	−4.1	−4.3	−3.7	−3.8
	ΔΔ	8.2	13.2	11.3	16.1

[a] Results for four protonation/redox microstates of the cluster are presented: oxidized and doubly protonated (ox, prot), reduced with the reducing electron formally placed at the histidine-coordinated iron and doubly protonated (redH, prot), oxidized and doubly deprotonated (ox, deprot), reduced with the reducing electron formally placed at the histidine-coordinated iron and doubly deprotonated (redH, deprot). The ΔΔ rows list the difference between the respective values for bc1R and FdR as $\Delta\Delta = \Delta G(\text{FdR}) - \Delta G(\text{bc1R})$.

Focusing on the differences between bc1R and FdR, it is evident from our calculations that the differences in transfer energy are exclusively due to the differences in the background energy. The Born energy is essentially the same for both proteins. These results provide further evidence against the solvent-exposure hypothesis (*6*, *33*), which was used to explain the differences in pH dependence of the reduction potential of *bc*-type and ferredoxin Rieske proteins before their structures were known. In fact, the influence of the distribution of dielectric boundaries in the protein/solvent environment is essentially identical in bc1R and FdR, as obvious from the neglectable differences in ΔG_{Born}. In contrast, the differences in chemical behavior of the cluster are exclusively due to differences between the charge distributions of the proteins.

Effects of Mutations. To identify structural differences between bc1R and FdR that account for the differences between their pK_a values, we have performed calculations on a set of mutants of both proteins. The investigated mutations were chosen to remove electrostatic differences between the two structures. In bc1R, hydrogen bonds toward the cluster were removed. In FdR, negatively charged residues were neutralized. A disulfide bridge connecting the two cluster binding loops in *bc*-type but not ferredoxin Rieske proteins has previously been shown to have no direct effect on the chemical behavior of the cluster (*34*, *35*). The studied mutations allow us to relate structural differences between bc1R and FdR to differences in their physical properties.

Mutations of the Hydrogen-Bonding Pattern in bc1R. In bc1R, we have studied mutations that remove two of the hydrogen bonds in the vicinity of the cluster. The side-chain hydroxyl groups of Ser163 and Tyr165 make hydrogen bonds with one of the core sulfur atoms and the sulfur atom of the

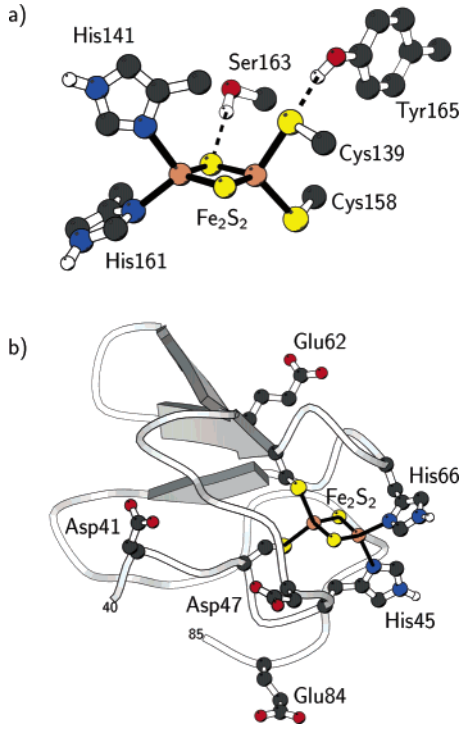

FIGURE 4: Structural features of the cluster environment in bc1R and FdR that have been studied mutationally. Nonpolar hydrogen atoms have been omitted for clarity. Panel a shows hydroxyl side chains acting as hydrogen bond donors toward the Rieske cluster in bc1R (*8*). The [Fe_2S_2] core, ligand side chains, and the hydrogen bond donors Ser163 and Tyr165 are shown. Hydrogen bonds are depicted as dashed lines. Panel b shows the structure of the cluster binding domain of FdR (*7*). The Rieske cluster and studied negatively charged residues are highlighted.

Table 3: Calculated Macroscopic pK_a Values for Wild-Type and Mutant bc1R

	pK_a values			
	oxidized		reduced	
wild-type	7.9	9.2	10.8	13.7
S163A	8.4	9.6	11.2	14.1
Y165F	8.1	9.3	10.9	13.8

iron-ligand Cys139, respectively (see Figure 4a). No equivalent hydrogen bonds are present in FdR. Ser163 and Tyr165 are conserved among all *bc*-type Rieske proteins, with the exception of Rieske proteins from menaquinol-oxidizing complexes that replace Ser163 with alanine or glycine. We investigated the mutations S163A and Y165F that have also been characterized experimentally (*36*−*38*).

Our calculations show that the ligand histidine pK_a values are higher in the mutants than in the wild-type protein (see Table 3): removal of the hydrogen bonds results in destabilization of states with higher charge densities, which are the deprotonated states. The more pronounced effect of the S163A mutation compared to the effect of the Y165F mutation has also been observed experimentally for shifts of the cluster reduction potential induced by these mutations (*36*, *37*). Experimentally determined pK_a values of the Y165F mutant in *Rb. sphaeroides* differ only within experimental error from those of the wild-type protein (*38*). This result agrees well with the small effect of this mutation on the pK_a values observed in the calculations.

Table 4: Calculated Macroscopic pK_a Values for Wild-Type and Mutant FdR

	pK_a values			
	oxidized		reduced	
wild-type	9.1	9.8	12.2	14.5
D41N	8.7	9.3	11.7	13.9
D47N	8.8	9.5	12.1	14.3
E62Q	8.6	9.2	11.9	14.0
E84Q	8.7	9.3	11.6	14.0
fourfold mutant D41N, D47N, E62Q, E84Q	8.1	8.7	11.1	13.4

Mutation of Negatively Charged Residues in FdR. The cluster environments of bc1R and FdR differ not only in their hydrogen-bonding patterns but also in the distribution of negatively charged residues in the vicinity of the cluster. We have changed the carboxylic residues Asp41, Asp47, Glu62, and Glu84 of FdR (see Figure 4b) to their amide counterparts asparagine and glutamine. The distance between the negatively charged residues and the histidine ligands are 15.8 Å for Asp41, 12.1 Å for Asp47, 11.3 Å for Glu62, and 9.4 Å for Glu84 (measured as distance between the closest carboxyl oxygen and the closest Nϵ-atom of the histidine ligands). The protonation state of the carboxylic residues in the wild-type structure of FdR has been determined by a Monte Carlo titration calculation, as has been described previously for bc1R (*5*): all four residues are negatively charged at physiological pH, irrespective of the state of the cluster.

The four single mutants D41N, D47N, E62Q, and E84Q lower the histidine pK_a values with respect to the wild-type by approximately the same amount (see Table 4). Removal of the negative charges around the cluster results in stabilization of cluster states with high negative charge densities, which are the deprotonated states. In addition to the four single mutants, we have studied their combination in a fourfold mutant as shown in Table 4. In the fourfold mutant, the histidine pK_a values are strongly shifted toward lower values.

The Structural Basis of the Differences in Titration Behavior and Their Functional Implication. From the calculations on mutations of both bc1R and FdR, we can conclude which structural differences account for the differences in their titration behavior. In the wild-type, bc1R has lower pK_a values than FdR (see Table 1). Mutational removal of two hydrogen bonds toward the cluster raises the pK_a values of bc1R (see Table 3). Mutational removal of negative charges around the cluster lowers the pK_a values of FdR (see Table 4). The effects of mutations S163A in bc1R and D41N, D47N, E62Q, and E84Q in FdR taken together can compensate completely for the observed difference between the wild-type pK_a values of bc1R and FdR (see Table 5). We can thus conclude that the absence of negatively charged side-chains around the cluster, in combination with the presence of hydrogen-bonds toward the cluster in bc1R are responsible for its lower pK_a values in comparison with FdR.

The charge-stabilizing effect of hydrogen bonds toward the cluster has been demonstrated in previous mutational studies measuring the cluster reduction potential (*36*−*38*). Here, we observe an equivalent effect of hydrogen-bond donors on the titration behavior of the ligand histidines. In

Table 5: A Combination of the Investigated Structural Differences between bc1R and FdR Can Account Completely for the Observed Differences in the Ligand Histidine pK_a values[a]

	ΔpK_a			
	oxidized		reduced	
wild-type pK_a values are **lower** in bc1R than FdR by	1.2	0.6	1.4	0.8
bc1R S163A shifts pK_a **up** by	0.5	0.4	0.4	0.4
FdR D41N, D47N, E62Q, and E84Q shift pK_a **down** by	1.0	1.1	1.1	1.1
sum of mutational pK_a shifts	1.5	1.5	1.5	1.5

[a] The uppermost row lists the difference between calculated wild-type pK_a values, which are lower for bc1R than for FdR. Since the studied mutations were chosen to remove electrostatic differences between bc1R and FdR, the pK_a values of the mutants are more similar than the pK_a values of the wild-type proteins. Adding up the effect of the mutation in bc1R (which raises the pK_a values with respect to the wild-type) and the effect of mutations in FdR (which lower the pK_a values with respect to the wild-type) demonstrates that the difference between the wild-type pK_a values of bc1R and FdR can be removed by the studied mutations.

addition, we could show that the presence of charged residues, which has not been considered earlier, has a large effect on the chemical behavior of the cluster. The effect of the charged residues on the pK_a values is larger than that of the hydrogen bonds toward the cluster. As can be seen from Table 5, the effect of charged residues is almost sufficient to explain the observed differences between the pK_a values of wild-type bc1R and FdR.

In *bc*-type Rieske proteins, the low pK_a values of the histidine cluster ligands provide the physical basis for the catalytic function of these proteins. The corresponding fact that the reduction potential depends on pH in the physiological range allows for coupled electron and proton uptake by the Rieske cluster. Such coupled electron and proton uptake has been proposed to be of functional importance in cytochrome bc_1 and b_6f complexes (*39*): the Rieske cluster of these enzyme complexes has been suggested to serve not only as electron but also as proton acceptor in the oxidation of quinol.

CONCLUSIONS

In the presented study, structural differences between a *bc*-type and a ferredoxin Rieske protein have been identified that account for the differences in the titration behavior of their identical Rieske iron−sulfur clusters. Our analysis of the results from Poisson−Boltzmann calculations confirms that the different charge distributions of the two proteins and not the degree of solvent exposure of the cluster is responsible for the experimentally observed differences in titration behavior. The experimental results could be well reproduced by our calculations. By mutational changes, electrostatic differences between the two studied proteins were eliminated. In the *bc*-type protein, hydrogen bonds toward the cluster were removed. In the ferredoxin Rieske protein, negative charges in the vicinity of the cluster were neutralized. The clusters of the *bc*-type and ferredoxin Rieske proteins behave more similarly in the mutated protein environments than in the wild-type proteins. A quantitative analysis indicates that presence of hydrogen bonds toward the cluster and absence of negatively charged side chains in the vicinity of the cluster account for the lower pK_a values of the iron-coordinating histidines in the *bc*-type Rieske protein. According to our calculations, the negative charges around the cluster have a larger effect on the pK_a values than the hydrogen bonds. The large effect of the negative charges in FdR predicted from our calculations can be tested experimentally. The differences in histidine pK_a values between the *bc*-type and the ferredoxin Rieske protein are the basis for the difference in pH dependence of their reduction potentials. The results presented here do thus provide a structural understanding of the pH dependence of the reduction potentials of *bc*-type Rieske proteins, which is of functional importance in all quinol-oxidizing cytochrome complexes.

ACKNOWLEDGMENT

We thank D. Bashford for providing his program MEAD, and E. J. Baerends and S. van Gisbergen for ADF.

SUPPORTING INFORMATION AVAILABLE

A detailed derivation of the relation between macroscopic and microscopic protonation equilibrium constants of the oxidized and reduced Rieske cluster. This material is available free of charge via the Internet at http://pubs.acs.org.

REFERENCES

1. Rieske, J. S., MacLennan, D. H., and Coleman, R. (1964) Isolation and properties of an iron-protein from the (reduced coenzyme Q)-cytochrome *c* reductase complex of the respiratory chain, *Biochem. Biophys. Res. Commun. 15*, 338−344.
2. Kuila, D., Schoonover, J. R., Dyer, R. B., Batie, C. J., Ballou, D. P., Fee, J. A., and Woodruff, W. H. (1992) Resonance Raman studies of Rieske-type proteins, *Biochim. Biophys. Acta 1140*, 175−183.
3. Iwasaki, T., Imai, T., Urushiyama, A., and Oshima, T. (1996) Redox-linked ionization of sulredoxin, an archeal Rieske-type [2Fe-2S] protein from *Sulfolobus sp.* strain 7, *J. Biol. Chem 271*, 27659−27663.
4. Link, T. A. (1997) The role of the 'Rieske' iron sulfur protein in the hydroquinone oxidation (Q_P) site of the cytochrome bc_1 complex. The proton gated affinity change mechanism, *FEBS Lett. 412*, 257−264.
5. Ullmann, G. M., Noodleman, L., and Case, D. A. (2002) Density functional calculation of the pK_a values and redox potentials in the bovine Rieske iron−sulfur protein, *J. Biol. Inorg. Chem. 7*, 632−639.
6. Link, T. A. (1999) The structures of Rieske and Rieske-type proteins, *Adv. Inorg. Chem. 47*, 83−157.
7. Colbert, C. L., Couture, M. M.-J., Eltis, L. D., and Bolin, J. T. (2000) A cluster exposed: structure of the Rieske ferredoxin from biphenyl dioxygenase and the redox properties of Rieske Fe−S proteins, *Structure 8*, 1267−1278.
8. Iwata, S., Saynovits, M., Link, T. A., and Michel, H. (1996) Structure of a water soluble fragment of the Rieske iron−sulfur protein of the bovine heart mitochondrial cytochrome bc_1 complex determined by MAD phasing at 1.5 Å resolution, *Structure 4*, 567−579.
9. Ullmann, G. M., and Knapp, E.-W. (1999) Electrostatic models for computing protonation and redox equilibria in proteins, *Eur. Biophys. J. 28*, 533−551.
10. Onufriev, A., Case, D. A., and Ullmann, G. M. (2001) A novel view of pH titration in biomolecules, *Biochemistry 40*, 3413−3419.
11. Li, H., Hains, A., Everts, J., Robertson, A. D., and Jensen, J. H. (2002) The prediction of protein pK_as using QM/MM: the pK_a of lysine 55 in turkey ovomucoid third domain, *J. Phys. Chem. B 106*, 3486−3494.
12. Reiss, H. and Heller, A. (1985) The absolute potential of the standard hydrogen electrode: a new estimate, *J. Phys. Chem. 89*, 4207−4213.
13. Li, J., Fisher, C. L., Chen, J. L., Bashford, D., and Noodleman, L. (1996) Calculation of redox potentials and pK_a values of

hydrated transition metal cations by a combined density functional and continuum dielectric theory, *Inorg. Chem. 35*, 4694−4702.
14. Klotz, I. M. (1997) *Ligand−receptor energetics*, Wiley, New York.
15. Ullmann, G. M. (2003) Relations between protonation constants and titration curves in polyprotic acids: A critical view, *J. Phys. Chem. B 107*, 1263−1271.
16. Zu, Y., Couture, M. M.-J., Kolling, D. R. J., Crofts, A. R., Eltis, L. D., Fee, J. A., and Hirst, J. (2003) Reduction potentials of Rieske clusters: importance of the coupling between oxidation state and histidine protonation state, *Biochemistry 42*, 12400−12408.
17. Guerra, C. F., Snijders, J. G., te Velde, G., and Baerends, E. J. (1998) Towards an order-*N* DFT method, *Theor. Chem. Acc. 99*, 391−403.
18. Vosko, S. H., Wilk, L., and Nusair, M. (1980) Accurate spin-dependent electron liquid correlation energies for local spin density calculations: a critical analysis, *Can. J. Phys. 58*, 1200−1211.
19. Perdew, J. P., Chevary, J. A., Vosko, S. H., Jackson, K. A., Pederson, M. R., Singh, D. J., and Fiolhais, C. (1992) Atoms, molecules, solids, and surfaces: applications of the generalized gradient approximation for exchange and correlation, *Phys. Rev. B 15*, 6671−6687.
20. Breneman, C. M., and Wiberg, K. B. (1990) Determining atom-centered monopoles from molecular electrostatic potentials. The need for high spin sampling density in formamide conformational analysis, *J. Comput. Chem. 11*, 361−373.
21. Mouesca, J.-M., Chen, J. L., Noodleman, L., Bashford, D., and Case, D. A. (1994) Density functional/Poisson−Boltzmann calculations of redox potentials for iron−sulfur clusters, *J. Am. Chem. Soc. 116*, 11898−11914.
22. Bondi, A. (1964) van der Waals volumes and radii, *J. Phys. Chem. 68*, 441−451.
23. Hill, T. (1960) *An introduction to statistical thermodynamics*, Addison-Wesley, Reading, Massachusetts.
24. MacKerell, A. D., Bashford, D., Bellott, M., Dunbrack, R. L., Jr., Evanseck, J. D., Field, M. J., Fischer, S., Gao, J., Guo, H., Ha, S., Joseph-McCarthy, D., Kuchnir, L., Kuczera, K., Lau, F. T. K., Mattos, C., Michnick, S., Ngo, T., Nguyen, D. T., Prodhom, B., Reiher, W. E., Roux, B., Schlenkrich, M., Smith, J. C., Stote, R., Straub, J., Watanabe, M., Wiorkiewicz-Kuczera, J., Yin, D., and Karplus, M. (1998) All-atom empirical potential for molecular modeling and dynamics studies of proteins, *J. Phys. Chem. B 102*, 3586−3616.
25. Bashford, D., and Karplus, M. (1990) pK_as of ionizable groups in proteins: atomic detail from a continuum electrostatic model, *Biochemistry 29*, 10219−10225.
26. Link, T. A. (1994) Two p*K* values of the oxidized Rieske [2Fe-2S] cluster observed by CD spectroscopy, *Biochim. Biophys. Acta 1185*, 81−84.
27. Baymann, F., Robertson, D. E., Dutton, P. L., and Mäntele, W. (1999) Electrochemical and spectroscopic investigations on the cytochrome bc_1 complex from *Rhodobacter capsulatus*, *Biochemistry 38*, 13188−13199.
28. Carrell, C. J., Zhang, H., Cramer, W. A., and Smith, J. L. (1997) Biological identity and diversity in photosynthesis and respiration: structure of the lumen-side domain of the chloroplast Rieske protein, *Structure 5*, 1613−1625.
29. Kauppi, B., Lee, K., Carredano, E., Parales, R. E., Gibson, D. T., Eklund, H., and Ramaswamy, S. (1998) Structure of an aromatic-ring-hydroxylating dioxygenase−naphthalene 1,2-dioxygenase, *Structure 6*, 571−586.
30. Ellis, P. J., Conrads, T., Hille, R., and Kuhn, P. (2001) Crystal structure of the 100 kDa arsenite oxidase from *Alcaligenes faecalis* in two crystal forms at 1.64 and 2.03 Å, *Structure 9*, 125−132.
31. Bönisch, H., Schmidt, C. L., Schäfer, G., and Ladenstein, R. (2002) The structure of the soluble domain of an archeal Rieske iron−sulfur protein at 1.1 Å resolution, *J. Mol. Biol. 319*, 791−805.
32. Hunsicker-Wang, L. M., Heine, A., Cheng, Y., Luna, E. P., Todaro, T., Zhang, Y. M., Williams, P. A., McRee, D. E., Hirst, J., Stout, C. D., and Fee, J. A. (2003) High-resolution structure of the soluble respiratory Rieske protein from *Thermus thermophilus*: analysis and comparison, *Biochemistry 42*, 7303−7317.
33. Link, T. A., Hatzfeld, O. M., Unalkat, P., Shergill, J. K., Cammack, R., and Mason, J. R. (1996) Comparison of the Rieske [2Fe-2S] center in the bc_1 complex and in bacterial dioxygenases by circular dichroism spectroscopy and cyclic voltammetry, *Biochemistry 35*, 7546−7552.
34. Zu, Y., Fee, J. A., and Hirst, J. (2002) Breaking and reforming the disulfide bond at the high-potential, respiratory-type Rieske [2Fe-2S] center of *Thermus thermophilus*: characterization of the sulfhydryl state by protein-film voltammetry, *Biochemistry 41*, 14054−14065.
35. Merbitz-Zahradnik, T., Zwicker, K., Nett, J. H., Link, T. A., and Trumpower, B. L. (2003) Elimination of the disulfide bridge in the Rieske iron−sulfur protein allows assembly of the [2Fe-2S] cluster into the Rieske protein but damages the ubiquinol oxidation site in the cytochrome bc_1 complex, *Biochemistry 42*, 13637−13645.
36. Denke, E., Merbitz-Zahradnik, T., Hatzfeld, O. M., Snyder, C. H., Link, T. A., and Trumpower, B. L. (1998) Alteration of the midpoint potential and catalytic activity of the Rieske iron−sulfur protein by changes of amino acids forming hydrogen bonds to the iron−sulfur cluster, *J. Biol. Chem. 273*, 9085−9093.
37. Schröter, T., Hatzfeld, O. M., Gemeinhardt, S., Korn, M., Friedrich, T., Ludwig, B., and Link, T. A. (1998) Mutational analysis of residues forming hydrogen bonds in the Rieske [2Fe-2S] cluster of the cytochrome bc_1 complex in *Paracoccus denitrificans*, *Eur. J. Biochem. 255*, 100−106.
38. Guergova-Kuras, M., Kuras, R., Ugulava, N., Hadad, I., and Crofts, A. R. (2000) Specific mutagenesis of the Rieske iron−sulfur protein in *Rhodobacter sphaeroides* shows that both the thermodynamic gradient and the p*K* of the oxidized form determine the rate of quinol oxidation by the bc_1 complex, *Biochemistry 39*, 7436−7444.
39. Crofts, A. R., Hong, S., Ugulava, N., Barquera, B., Gennis, R., Guergova-Kuras, M., and Berry, E. A. (1999) Pathways for proton release during ubihydroquinone oxidation by the bc_1 complex, *Proc. Natl. Acad. Sci. U.S.A. 96*, 10021−10026.

BI0488606